SDC-92-214

SDC
SOLENOIDAL DETECTOR NOTES

GENERAL MUON RESOLUTION CALCULATIONS

January 23, 1992

Jim Wiss
University of Illinois

Jim Wiss

January 23, 1992

General Muon Resolution Calculations

This note describes the calculational techniques employed by my new computer program which computes the muon track parameter resolution for a wide variety of track fits using a diversity of different magnet and detector geometries. This work was motivated by the desire to properly combine information from the central and intermediate tracker system and the barrel and forward muon system as a continuous function of η. General ways of handling diverse magnet geometries, multiple coulomb scattering layouts, and beam constraints are described and illustrated. The techniques describe linearized fits which operate to first order $1/P_t$.

1. Track Parameters , Linearization, and Beam Constraints

I begin by describing one of the more fundamental but subtle aspects of my approach – the specification of track parameters, the linearization assumptions, and the scheme used for the incorporation of beam constraint information.

The detectors in the usual magnetic spectrometer measure the space points of a track downstream of its origin. Hence spectrometers measure the *trajectory* of a given track which can be specified from the 3-momenta, and spacial coordinates at some **arbitrary** reference time (or path length). The single track fit provided by the usual spectrometer (in the absence of beam constraint information) cannot determine the absolute origin of the track. The arbitrariness of the reference time measured by a spectrometer means that the standard track is specified by 5 rather than 6 parameters. On the other hand, a beam constraint provides information on the origin as well as track trajectory and fits utilizing this constraint can specify all 6 parameters of a track. This section describes the way the problem of two track parameterizations is handled in the resolution program.

We begin by describing the track parameter set used in the absence of beam constraint information. For a collider detector, the θ and ϕ angles of momentum

vector are a natural choice of parameters to describe the local direction of the particle as near as possible to the global event vertex. Since magnetic deflections tend to depend to lowest order on Q/P_t or Q/P either or these "curvature" variables are a good choice to describe the charged momentum magnitude in a linearized fit. My program provides a choice of either curvature definition and results do not appear to depend on the choice to any observable extent.

Now on to the more subtle problem of specifying impact parameter information for the case of no beam constraint where only trajectories are measured. Locally the track trajectory is, to zero order in $1/P$, a straight line directed along the $\hat{p}$ direction and passing through the point $\vec{I}$. The trajectory as a function of path length s is given by

$$\vec{X} = \vec{I} + (s - s_o)\,\hat{p}$$

where s_o is the arbitrary reference path length. The arbitrariness in reference path length implies that $\vec{I}$ component along $\hat{p}$ direction is arbitrary. A natural way to specify $\vec{I}$ is to specify the two, non-arbitrary $\vec{I}$ components which are transverse to $\hat{p}$. A natural choice of transverse directions are the $\hat{\phi}$ and $\hat{\theta}$ unit vectors. $\vec{I} = I_\phi\hat{\phi} + I_\theta\hat{\theta}$... where

$\hat{p}$	$(\,S_\theta C_\phi \quad S_\theta S_\phi \quad C_\theta\,)$
$\hat{\theta}$	$(\,C_\theta C_\phi \quad C_\theta S_\phi \quad -S_\theta\,)$
$\hat{\phi}$	$(\,-S_\phi \quad C_\phi \quad 0\,)$

$$S_\phi \equiv sin\phi \quad C_\phi \equiv cos\phi \quad S_\theta \equiv sin\theta \quad C_\theta \equiv cos\theta$$

Hence our choice of track parameters is:

Track Parameters for Fits without Beam Constraints

1	2	3	4	5
Q/P or Q/P_t	ϕ	θ	$\hat{\phi}\cdot\vec{I}$	$\hat{\theta}\cdot\vec{I}$

Beam Constraints

To set the stage, we begin with some general comments about linear fitting. In a linear fit, the predicted value of the measured coordinates (w_i) are written as the track parameters (t_α) times a transport matrix ($T_{i\alpha}$) or $w_i = T_{i\alpha}\ t_\alpha$. In a linearized fits, this relation is of the differential form: $\partial w_i = T_{i\alpha}\ \partial t_\alpha$. To lowest order in Q/P the transport matrix elements are functions of (ϕ θ) alone and depend on the detector and magnetic geometry. General expressions for $T_{i\alpha}$ are obtained in Sections 2 for arbitrary detector geometries and magnetic field deployments.

One fits for the track parameters by minimizing a χ^2 given by :

$$\chi^2 = C_{ij}^{-1}\left(w_i - T_{i\alpha}t_\alpha\right)\left(w_j - T_{j\beta}t_\beta\right) \tag{1}$$

where: $C_{ij} =< \delta w_i\ \delta w_j >$ is the coordinate covariance matrix reflecting multiple scattering as well as measurement contributions. General expressions for the multiple scattering contributions are given in Section 3. The error matrix describing the covariance matrix of the track parameters for the fitted parameter is the reciprocal of the fit matrix (H) which has components:

$$H_{\alpha\beta} = C_{ij}^{-1}\ T_{i\alpha}\ T_{j\beta}$$

What are the transport matrix elements appropriate to the beam constraint? The beam constraint provides additional information on the impact parameter based fit parameters by relating tracks to the interaction point ($\vec{X}$). In the absence of measurement error (or finite decay length), we expect:

$$\vec{X} = \sum_\alpha I_\alpha\ \hat{u}^\alpha$$

where the α runs over the three dimensions, $I_{1,2}$ are the fourth and fifth track parameters, I_3 is a new, 6th parameter which specifies the path length to the

track origin in a way hopefully, consistent with the beam constraint. The unit direction vectors are:

$$\hat{u}^{(1)} = \hat{\phi} \ , \ \ \hat{u}^{(2)} = \hat{\theta} \ , \ \ \hat{u}^{(3)} = \hat{p}$$

The beam constraint information can be incorporated in the fit through the inclusion of an additional χ^2 contribution of the form:

$$\chi^2_{bc} = C^{-1}_{mn} \left(I_\alpha u^\alpha_m - X_m \right) \left(I_\beta u^\beta_n - X_n \right) \tag{2}$$

where $C_{mn} =< \delta X_m \ \delta X_n >$ is the covariance matrix describing the beam interaction point. Comparing the χ^2 expressions of Eqn. (1) and (2), we conclude that the beam constraint can be incorporated into the fit by including a sixth fit parameter I_3, and using a transport matrix given by $T_{i\alpha} = \hat{u}^\alpha_i$. The T_{i6} is only nonzero for the beam constraint measurements (eg $i = 1 \rightarrow 3$)

Track Parameters for Fits with Beam Constraints

1	2	3	4	5	6
Q/P or Q/P$_t$	ϕ	θ	$\hat{\phi} \cdot \vec{I}$	$\hat{\theta} \cdot \vec{I}$	$\hat{p} \cdot \vec{I}$

In previous incarnations of my resolution program, the beam constraint was modeled as two "chamber" systems at zero radius – one measuring the $\hat{\phi}$ coordinate (with typically 20 μ resolution) and one measuring the $\hat{z}$ coordinate with either 1 mm or 5 cm resolution (depending on whether or not the fit is in a triggering or off line context). Only 5 fit parameters are used in the previous program. The results using the previous (and over simplified) approach appear nearly identical the results using the approach advocated here, except the momentum resolution becomes ϕ dependent if the X and Y beam constraint resolutions are not assumed to be identical.

2. General Transport Matrix Elements

The program assumes that the i'th detector measures some specified component (w_i) along a read-out direction ($\hat{w}_i$) of the intersection of tracks with local detector planes (whose normal and position may well be a function of the track polar angles). The set of w_i represent the actual coordinates which are fitted to provide the track parameters. The transport matrix element is given by the derivative of w_i with respect to the α'th track parameter (t_α): $T_{i\alpha} = \partial w_i / \partial t_\alpha$. Denoting the track intersection point in the i'th detector plane $\vec{x}_i$ we thus have $w_i = \hat{w}_i \cdot \vec{x}_i$.

In the absence of deflections (either magnetic or due to multiple scattering), the intersection of a track passing through point $\vec{Y}$ and directed along $\hat{p}$ with a detector plane which contains the point $\vec{d}_i$ and has a local normal η_i is:

$$\vec{x}_i = \vec{Y} + \frac{\hat{\eta}_i \cdot \left(\vec{d}_i - \vec{Y}\right)}{\hat{p} \cdot \hat{\eta}_i} \hat{p}$$

It is straightforward (and useful) to compute the derivatives of $w_i = \hat{w}_i \cdot \vec{x}_i$ with respect to either the track position ($\vec{Y}$) or direction ($\hat{p}$):

$$\partial w_i = \vec{g}_i \cdot \partial \vec{Y} \quad , \quad \partial w_i = \frac{\hat{\eta}_i \cdot \left(\vec{d}_i - \vec{Y}\right)}{\hat{p} \cdot \hat{\eta}_i} \vec{g}_i \cdot \partial \hat{p} \tag{3}$$

where the ubiquitous $\vec{g}_i$ vector depends on the read out direction and detector plane normal according to:

$$\vec{g}_i = \hat{w}_i - \frac{\hat{p} \cdot \hat{w}_i}{\hat{p} \cdot \hat{\eta}_i} \hat{\eta}_i \tag{4}$$

We are now well positioned to compute the transport elements in the high momentum limit for $t_{2,3}$ which describe how the measured coordinates depend on initial polar angle, and $t_{4,5}$ which describe how the measured coordinates depend on the position close to the origin. Lets begin with $t_{4,5}$ (and t_6 for fits with beam

constraint). The changes in the position near the origin due to changes in $t_{3\to 6}$ are

$$\partial\vec{Y} = \partial t_4\hat{\phi} + \partial t_5\hat{\theta} + \partial t_6\hat{p}$$

Hence:

$$T_{i4} = \vec{g}_i \cdot \hat{\phi} \quad , \quad T_{i5} = \vec{g}_i \cdot \hat{\theta} \quad , \quad T_{i6} = \vec{g}_i \cdot \hat{p} = 0 \tag{5}$$

It is easy to show $\vec{g}_i \cdot \hat{p} = 0$, thus strengthening our argument that a downstream detector provides no information t_6 which is the space coordinate component along the particle's momentum vector. hence the sixth track parameter is only meaningful when beam information is included in the fit.

Changes in track parameters t_2 (ϕ) and t_3 (θ) represents changes in the track direction $\hat{p}$ near (lets say at) the origin ($\vec{Y} = 0$).

$$\partial\hat{p} = t_2\ S_\theta\ \hat{\phi} + t_3\ \hat{\theta}$$

Hence:

$$T_{i2} = S_\theta\ \vec{g}_i \cdot \hat{\phi}\ \frac{\hat{\eta}_i \cdot \vec{d}_i}{\hat{p} \cdot \hat{\eta}_i} \quad , \quad T_{i3} = \vec{g}_i \cdot \hat{\theta}\ \frac{\hat{\eta}_i \cdot \vec{d}_i}{\hat{p} \cdot \hat{\eta}_i} \tag{6}$$

In the next section we give a general expression for the dispersion (D_i) where $\partial w_i = D_i\ \partial Q/P$.

Track Parameters and Transport Element Summary

	Parameter		Chamber	BC
1	Q/P	T_{i1}	D_i	0
2	ϕ	T_{i2}	$S_\theta\ \vec{g}_i \cdot \hat{\phi}\ \frac{\hat{\eta}_i \cdot \vec{d}_i}{\hat{p} \cdot \hat{\eta}_i}$	0
3	θ	T_{i3}	$\vec{g}_i \cdot \hat{\theta}\ \frac{\hat{\eta}_i \cdot \vec{d}_i}{\hat{p} \cdot \hat{\eta}_i}$	0
4	$\vec{I} \cdot \hat{\phi}$	T_{i4}	$\vec{g}_i \cdot \hat{\phi}$	$\hat{u}_i \cdot \hat{\phi}$
5	$\vec{I} \cdot \hat{\theta}$	T_{i5}	$\vec{g}_i \cdot \hat{\theta}$	$\hat{u}_i \cdot \hat{\theta}$
6	$\vec{I} \cdot \hat{p}$	T_{i6}	0	$\hat{u}_i \cdot \hat{p}$

$$g_i = \hat{w}_i - \frac{\hat{p} \cdot \hat{w}_i}{\hat{p} \cdot \hat{\eta}_i} \hat{\eta}_i$$

$$\hat{u}_1 = \hat{x} \quad , \quad \hat{u}_2 = \hat{y} \quad , \quad \hat{u}_3 = \hat{z}$$

Magnetic Dispersion

Let us assume that the track strikes a thin magnetic slab which we denote as the n'th magnetic slab at point $\vec{M}_n$. Let Δs_n be the path length traveled within the slab, and B_n and $\hat{b}_n$ be the magnitude and direction of the field within the slab. The field slab will deflect the track (charge Q , and momentum magnitude P) by an amount:

$$\partial \hat{p} = \frac{.3\ B_n\ Q}{P}\ \ \Delta s_n\ \ \hat{p} \times \hat{b}_n$$

Using Eqn. (3) and the definition of the dispersion we have:

$$D_i = \sum_n\ .3\ B_n\ \Delta s_n\ \ \frac{\hat{\eta}_i \cdot \left(\vec{d}_i - \vec{M}_n\right)}{\hat{p} \cdot \hat{\eta}_i}\ \vec{g}_i \cdot \left(\hat{p} \times \hat{b}_n\right) \tag{7}$$

where the sum runs over all magnetic slabs upstream of the i'th detector plane.

It is straightforward to show that Eqn. (7) applies to thick slabs (of constant field strength and direction) as long as $\vec{M}$ refers to the intersection at 1/2 the path length into the slab.

Recently by popular demand, I included an option to use the complete field map computed by Bob Wands of Fermilab which describes both the solenoid and flux return. Essentially the only change in Eqn. (7) required for a continuous rather than a slab field map is the replacement of $\sum_n \Delta s_n \rightarrow \int\ ds$, the replacement of $\vec{M}_n \rightarrow s\ \hat{p}$ and use the map to determine $\vec{B}(\vec{x}) = \vec{B}(s\ \hat{p})$. The implementation of the complete map, read in through a file and interpolated

with a CERNLIB interpolator made only the slightest differences in computed momentum resolution and resulted in only a very small difference in execution speed. I use as a default 1 cm steps in path length, s.

2. General Multiple Scattering Formalism

The coordinate covariance matrix is assumed to be of the form:

$$< \delta w_i \delta w_j > = C_{ij} = \sigma_i^2 \, \delta_{ij} + A_{ij}/P^2$$

where σ_i represents measurement error and A_{ij} represents correlated errors due to multiple scattering slabs upstream of both the i'th and j'th detector planes. We begin by talking about the scattering from very thin slabs and then discuss the modifications necessary for finite slabs.

Let us compute the anticipated correlation between the i'th and j'th coordinate due to a track which intercepts a multiple scattering plane at point $\vec{M}_n$. The track travels through a path length of size Δs_n and radiation length λ_n. The slab will create stochastic changes in $\hat{p}$.

$$< \delta \hat{p}_a \delta \hat{p}_b > = \left(\frac{.0141}{P} \right)^2 \frac{\Delta s_n}{\lambda_n} \, (\delta_{ab} - \hat{p}_a \hat{p}_b)$$

Here the $_a$ and $_b$ subscripts represent the Cartesian components of vectors. The structure $(\delta_{ab} - \hat{p}_a \hat{p}_b)$ says that the change in direction is statistically isotropic but $\perp$ to the initial direction $\hat{p}$.

Eqn. (3) can be used to relate the $< \delta \hat{p}_a \delta \hat{p}_b >$ which occurs at point $\vec{M}_n$ covariance matrix to the A matrix:

$$< \delta w_i \delta w_j > = \left(\frac{\hat{\eta}_i \cdot \left(\vec{d}_i - \vec{M}_n \right) \quad \hat{\eta}_j \cdot \left(\vec{d}_j - \vec{M}_n \right)}{\hat{p} \cdot \hat{\eta}_i \; \hat{p} \cdot \hat{\eta}_j} \right) \vec{g}_a^{(i)} < \delta \hat{p}_a \delta \hat{p}_b > \vec{g}_b^{(j)}$$

Putting it all together for thin slabs we have:

$$< \delta w_i \delta w_j >= \left(\frac{.0141}{P}\right)^2 \left(\frac{\vec{g}_i \cdot \vec{g}_j - \vec{g}_i \cdot \hat{p} \quad \vec{g}_j \cdot \hat{p}}{\hat{p} \cdot \hat{\eta}_i \; \hat{p} \cdot \hat{\eta}_j}\right) \mathcal{S}$$

$$\mathcal{S} = \sum_n \frac{\Delta s_n}{\lambda_n} \; \hat{\eta}_i \cdot \left(\vec{d}_i - \vec{M}_n\right) \; \hat{\eta}_j \cdot \left(\vec{d}_j - \vec{M}_n\right) \tag{8}$$

where the sum ($\mathcal{S}$) of Eqn (8) extends over all slabs which are upstream of both detector planes i and j.

It is useful to generalize the sum in Eqn. (8) to the case of thick slabs. We do this by considering each slab$_n$ as comprised as an infinite number of infinitesimal sub-slabs. The intersection of the track with the sub-slab is referenced with respect to the center of slab$_n$ ($\vec{M}_n$) and one integrates from $-\Delta s_n/2 \rightarrow \Delta s_n/2$.

$$\mathcal{S} = \sum_n T_n$$

where

$$T_n = \int_{-\Delta s_n/2}^{\Delta s_n/2} \frac{ds}{\lambda_n} \; \hat{\eta}_i \cdot \left(\vec{d}_i - \vec{M}_n - s\hat{p}\right) \; \hat{\eta}_j \cdot \left(\vec{d}_j - \vec{M}_n - s\hat{p}\right)$$

Performing the integral we obtain:

$$T_n = \frac{\Delta s_n}{\lambda_n} \left(\hat{\eta}_i \cdot \left(\vec{d}_i - \vec{M}_n\right) \; \hat{\eta}_j \cdot \left(\vec{d}_j - \vec{M}_n\right) + \frac{\hat{p} \cdot \eta_i \;\; \hat{p} \cdot \eta_j}{12} \Delta {s_n}^2\right)$$

Putting it all together we obtain:

$$C_{ij} = \sigma_i^2 + A_{ij}/P^2$$

$$A_{ij} = (.0141)^2 \left(\frac{\vec{g}_i \cdot \vec{g}_j - \vec{g}_i \cdot \hat{p} \quad \vec{g}_j \cdot \hat{p}}{\hat{p} \cdot \hat{\eta}_i \;\; \hat{p} \cdot \hat{\eta}_j}\right) \mathcal{S}$$

$$\mathcal{S} = \sum_n \frac{\Delta s_n}{\lambda_n} \left(\hat{\eta}_i \cdot \left(\vec{d}_i - \vec{M}_n \right) \; \hat{\eta}_j \cdot \left(\vec{d}_j - \vec{M}_n \right) + \frac{\hat{p} \cdot \eta_i \; \hat{p} \cdot \eta_j}{12} \Delta s_n{}^2 \right) \qquad (9)$$

3. Implementation

The program is set up to plot fractional resolutions, and momentum biases due to detector miss-alignment, and related quantities as a function of kinematic variables such as ϕ, η, and P_t. For a given (ϕ θ) choice, the program begins by making a reduced list of detectors , multiple scatters, and magnetic fields which the given track will actually intersect or partially intersect. The intersections are computed assuming straight line trajectories emanating from the origin.

The boundaries relevant to detectors, scattering materials, and magnetic fields are specified in terms of two sets of dimensional check variables. Each dimension is specified by a plane normal, and an inner and outer distance along this normal. Path lengths through materials and fields, important in the calculations of multiple scattering and magnetic deflection, are computed as the difference between the most downstream intersection of the inner dimensional planes and the most upstream intersection of the outer dimensional planes. Valid intersections have positive path lengths. We assume thin detectors, which are specified by one directed distance along the primary normal, and inner and outer directed distances along the secondary normal.

For convenience the normals can be specified in terms Cartesian or cylindrical unit vectors whose Cartesian coordinates depend on (ϕ θ). A very useful third option for the muon system is an octet symmetry option where vector components are specified in one octant and automatically rotated about $\hat{z}$ in multiples of $\pi/4$ depending on the which octant is appropriate for the given track's ϕ.

The Cartesian, cylindrical, and octet symmetry vector specification options options also apply to the specification of magnetic field directions. Each material slab carries a radiation length λ, each magnetic field carries a field strength and direction, and each detector carries a measurement resolution and readout

specification number which can be used to determine $\hat{w}_i$,and $\hat{\eta}_i$, as a function of (ϕ θ). In most cases, the detector plane normal η_i is the same as the primary boundary normal. One notable exception is the case of projective θ layers for the barrel muon system which is modeled as having a η_i with components that change continuously in θ and discretely (octet symmetry) in ϕ; whereas the boundary normal is constant in θ and uses the octet symmetry option in ϕ.

4. Examples

Our examples assume the Si cylinder , Si disk , and Straw tube CTD layout described in W. Ford's , November 24th, 1991 , entry in SDCNEWS in the TRACKING folder. This tracking system alone (with no help from the beam constraint or muon system) gives a relative momentum error, $\sigma(P_t)/P_t$, of 13.2 % at 1 TeV at $\eta = 0$ according to my program and an independent calculation by Bill Ford. Some of these calculations assume the existence of a gas microstrip Intermediate Tracking Detector described in a December 26, 1991 E-mail message by Mike Edwards. Here is a summary of information abstracted from Edwards' message.

1. 3 superlayers per end.
2. Each superlayer is 4 layers- 2 pure radial + u and v stereo at $\pm$ 10° to the radial.
3. Each superlayer 10 cm thick in Z.
4. Position resolution of each layer 150 microns
5. Positions

Superlayer	Mean Z	Inner Radius	Outer radius
1	2.90 m	0.35 m	1.12 m
2	3.40 m	0.41 m	1.31 m
3	3.90 m	0.47 m	1.50 m

Some calculations assume the existence of forward and barrel muon detectors. The barrel muon detectors use a 1.5 m thick toroid arranged in an octagonal box. We assume the box extends to $\eta = 1.55$. For historical reasons we use a barrel layout similar but not identical to that agreed to at the November 1991, SSCL SDC meeting. Specifically we assume we model BW1 as having two projective $\hat{\theta}$ doublets and two (non-projective) ϕ layer doublets. Each left-right resolving doublet has a combined measurement error of 250 μ. These calculation assume that BW2 and BW3 have just two $\hat{\theta}$ doublets and no $\hat{\phi}$ doublets.

The forward muon detector assumed in these calculations has 5 stations of chambers consisting 14 left-right resolving doublets. Each layer doublet has 150 μm resolution and 7.5^o stereo is assumed. We assume that the forward toroid is comprised of two 1.5 meter thick sections and use the inner and outer radius described in Bensinger's December 11, 1991 SDCNEWS entry in the MUON folder.

The forward muon system forms a set of octant pies, normal to the $\hat{z}$ axis which primarily measures momenta through the θ bend induced by the forward muon toroids. Within a given octant, three views are measured by the forward muon system, a $\hat{\rho}$ view along the octant bisector, and $\hat{s}_1$ and $\hat{s}_2$ views inclined at $\pm 7.5^o$ with respect to the octant bisector. My calculations assume the following deployment scheme for the left-right resolving doublets of the forward muon system.

	$Z_{\rm up}$	$Z_{\rm dwn}$	Views
FW1	7.06	7.49	$\hat{\rho}$, $\hat{\rho}$
FW2	8.69	9.59	$\hat{\rho}$, $\hat{s}_1$, $\hat{s}_2$, $\hat{\rho}$
FW3	11.27	11.70	$\hat{\rho}$, $\hat{\rho}$
FW4	13.38	14.04	$\hat{\rho}$, $\hat{\rho}$
FW5	16.34	17.24	$\hat{\rho}$, $\hat{s}_1$, $\hat{s}_2$, $\hat{\rho}$

Finally, I assume the outer radial edge of the forward muon system cuts off

at $\eta = 1.55$.

Figure 1 shows a plot of the relative momentum error $\sigma(P_t)/P_t$ as a function of η at a fixed $P_t = 1000\ GeV$. The solid curve is for a complete detector system with beam constraint, Si disk and cylinders, straw chamber CTD, gas microstrip, and forward and barrel muon detector. The detector boundaries in η are clearly and dramatically visible. A rather optimistic beam constraint is assumed of $20\mu m$ in X and Y and 300 μm in Z. The dashed curve has the beam constraint removed. With this very powerful system (especially in Si) the beam constraint is not that important. The dotted curve has the both the forward and barrel muon system removed. Clearly the forward muon system plays an important role in momentum resolution for $|\eta| > 1.3$ at $P_t = 1000\ GeV$. The gas microstrip system is not an important contributor to momentum resolution at $P_t = 1000\ GeV$ when used in conjunction with the forward muon system.

Figure 2 shows $\sigma(P_t)/P_t$ as a function of ϕ at a fixed $P_t = 1000\ GeV$ for $\eta = 0$ (solid) and $\eta = 1.7$ (dashed). A very small amount of ϕ dependence is observed which reflects the octagonal symmetry breaking effects discussed in my September 23, 1991 memo "Octagonal Geometry Effects" (SDCNOTE SDC-91-152). These effects include a ϕ dependence to the lever arm from the magnetic centroids to the muon detector planes, and the ϕ bending created by the octagonal barrel muon toroid. These features are automatically incorporated into my new program through the use of the general, lowest order expressions for the magnetic deflection and multiple scattering derived in Sections 2 and 3.

Figure 3 illustrates the handling of beam constraints in the new program. We illustrate the $\sigma(P_t)/P_t$ as a function of ϕ at a fixed $P_t = 1000\ GeV$ for an $\eta = 0$ track. The detector system includes the Si , and straw chamber CTD system described by Ford and for purposes of illustration we assume an azimuthally anisotropic knowledge of the beam. The solid curve assumes $(\sigma_X \quad \sigma_Y \quad \sigma_Z) = (20\ \mu m \quad 40\ \mu m \quad 5cm)$; the dashed curve assumes $(\sigma_X \quad \sigma_Y \quad \sigma_Z) = (20\ \mu m \quad 80\ \mu m \quad 5cm)$; and the dotted curve assumes

$(\sigma_X \quad \sigma_Y \quad \sigma_Z) = (20\ \mu m \quad 160\ \mu m \quad 5cm)$. The beam subtends the most transverse profile for tracks emerging near $\phi = 90^o$. For the new SDC detector, as opposed to the LOI detector, the beam constraint is not that important and this figure is only meant to illustrate this feature of my new program.

We conclude with Figure 4 which illustrates the use of the program in determining the effects of rigid body mis-alignment on momentum resolution. Figure 4 shows the resolution normalized momentum bias as a function of ϕ for the case of a fit which only uses information from the barrel muon system and hence determines momentum from the deflection of the barrel toroid. The particular example is for an $\eta = 1$, $P_t = 1000\ GeV$ muon and a system where BW1 is shifted by 1 mm in $\hat{x}$ relative to BW2 and BW3. A more complete description of mis-alignment calculations is presented in my November 10,1991 memo entitled "Muon System Alignment Studies" (SDCNOTE SDC-91-154)

Fig 1: PT = 1000

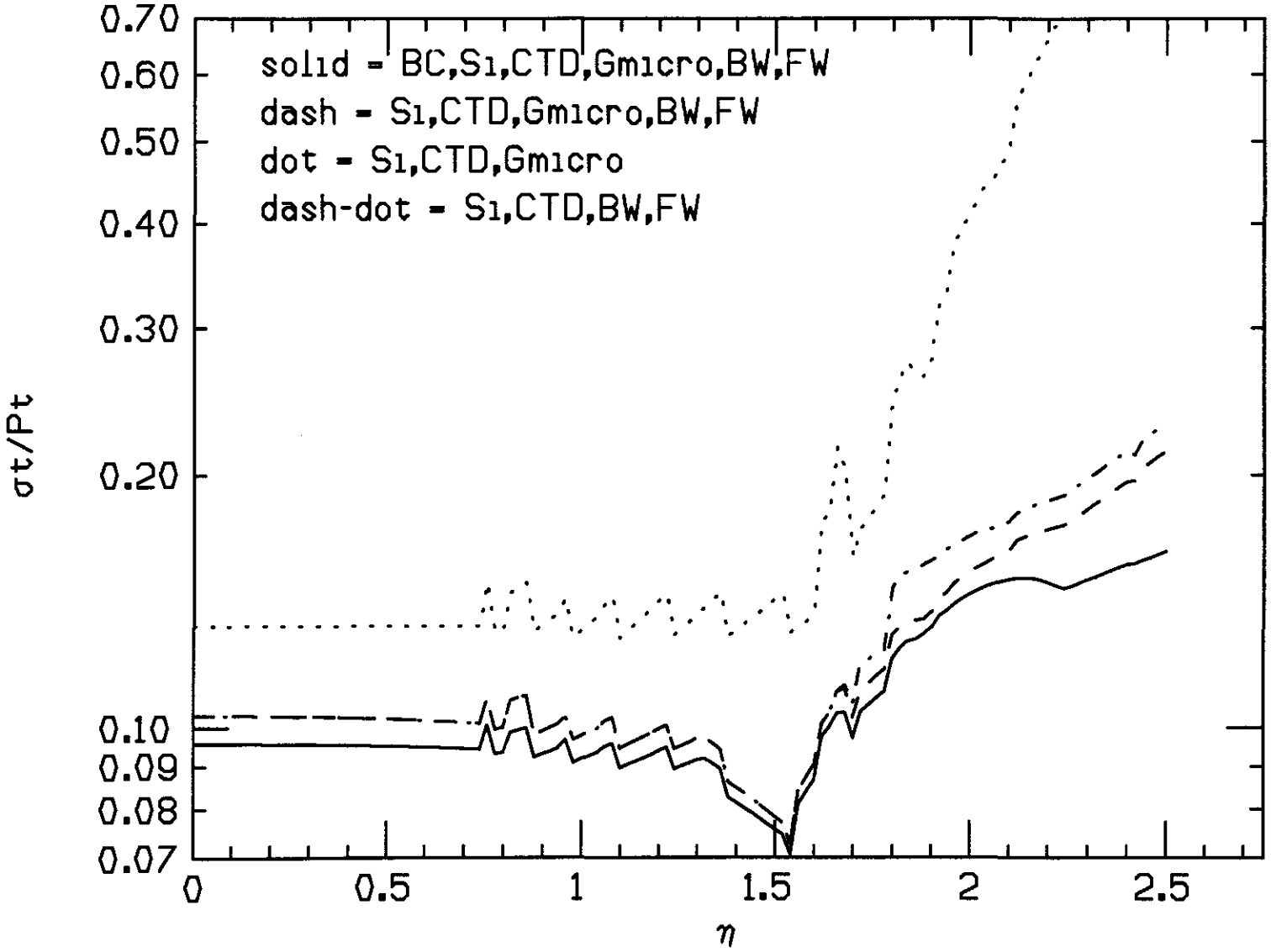
solid = BC,S1,CTD,Gmicro,BW,FW
dash = S1,CTD,Gmicro,BW,FW
dot = S1,CTD,Gmicro
dash-dot = S1,CTD,BW,FW
0.70
0.60
0.50
0.40
0.30
0.20
0.10
0.09
0.08
0.07
σt/Pt
0
0.5
1
1.5
2
2.5
η

Fig 2: Pt = 1000 S1,CTD,Gmicro,BW,FW

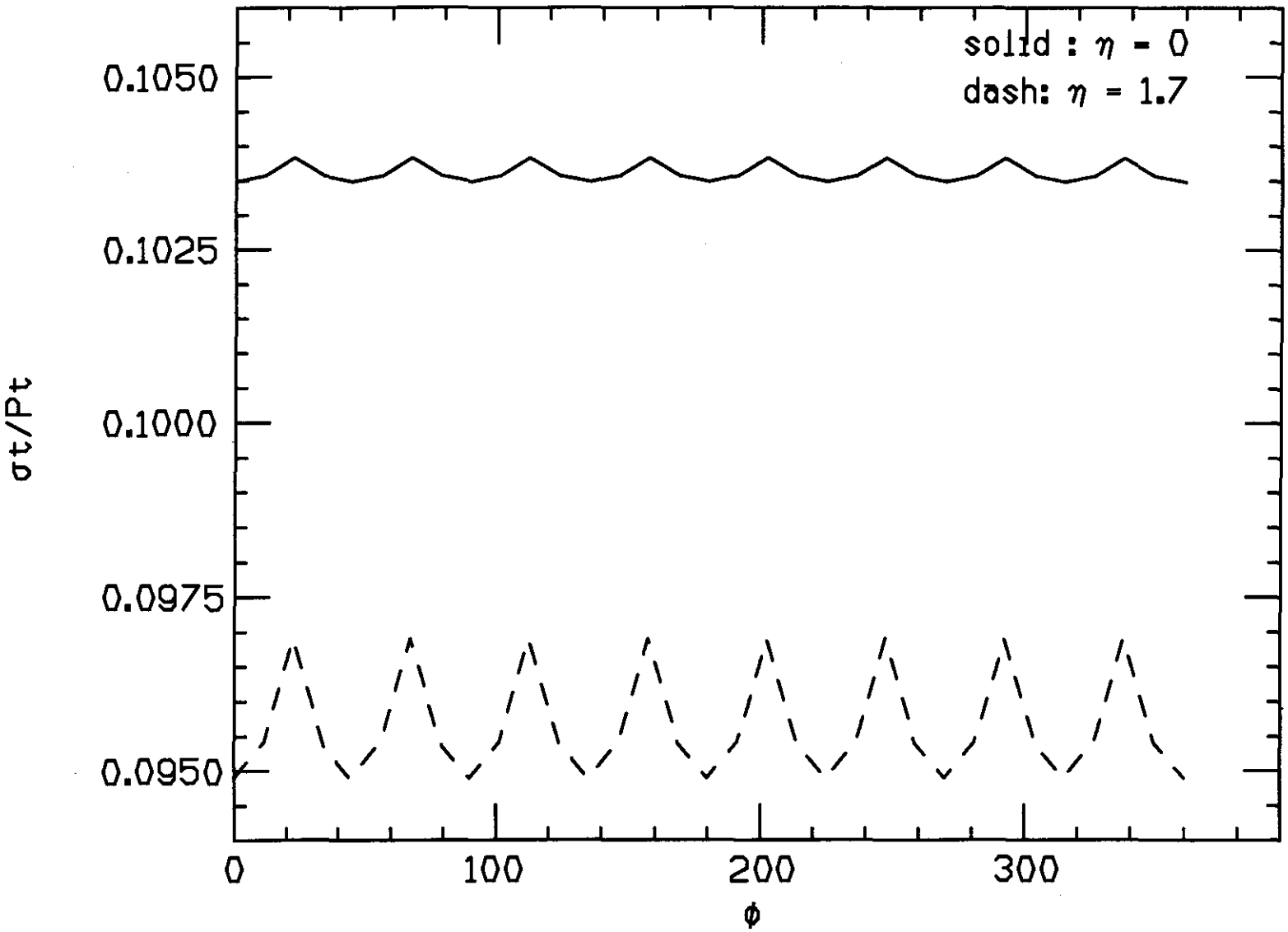

Fig 3: Pt = 1000 BC,Si,CTD

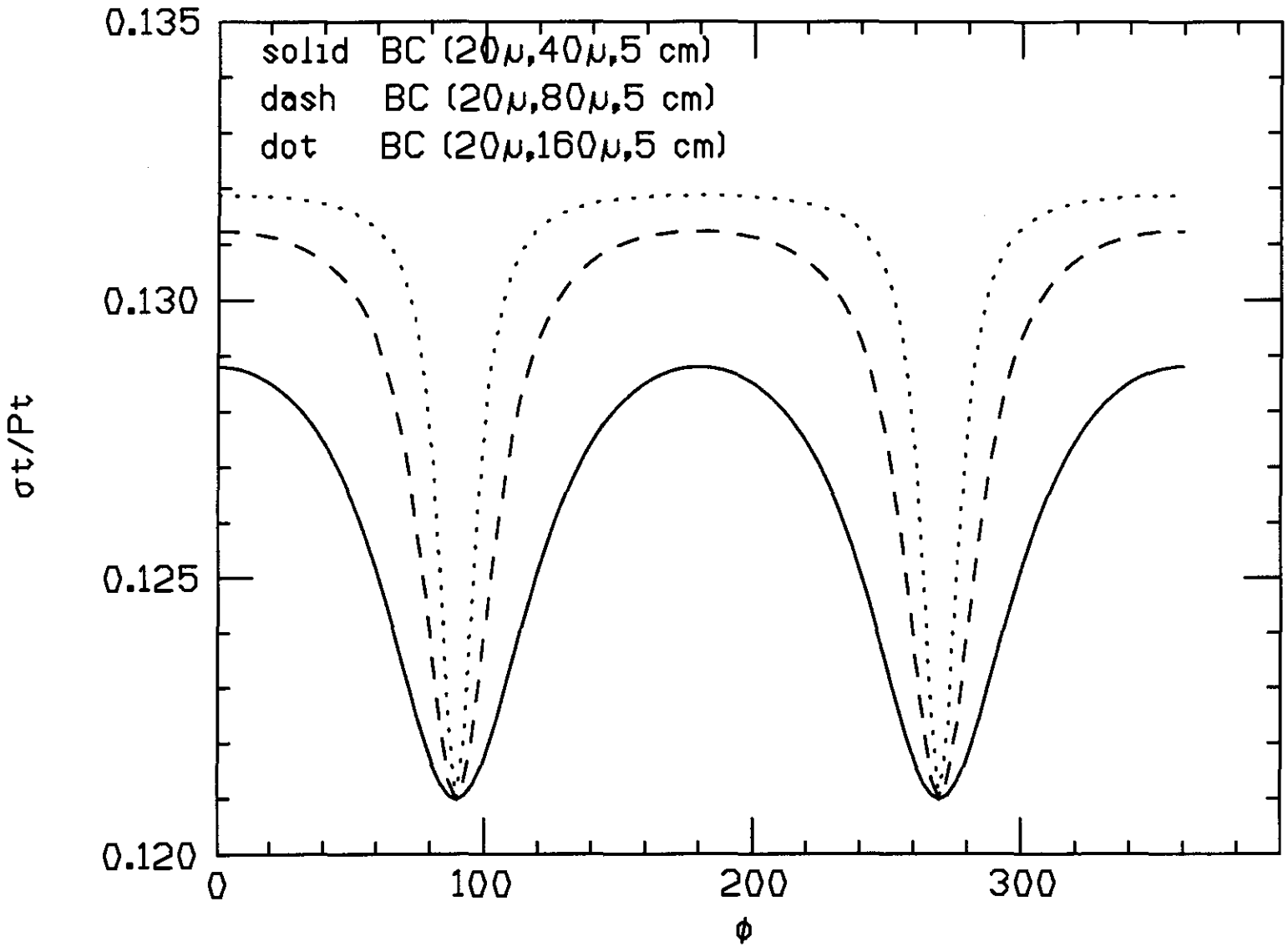
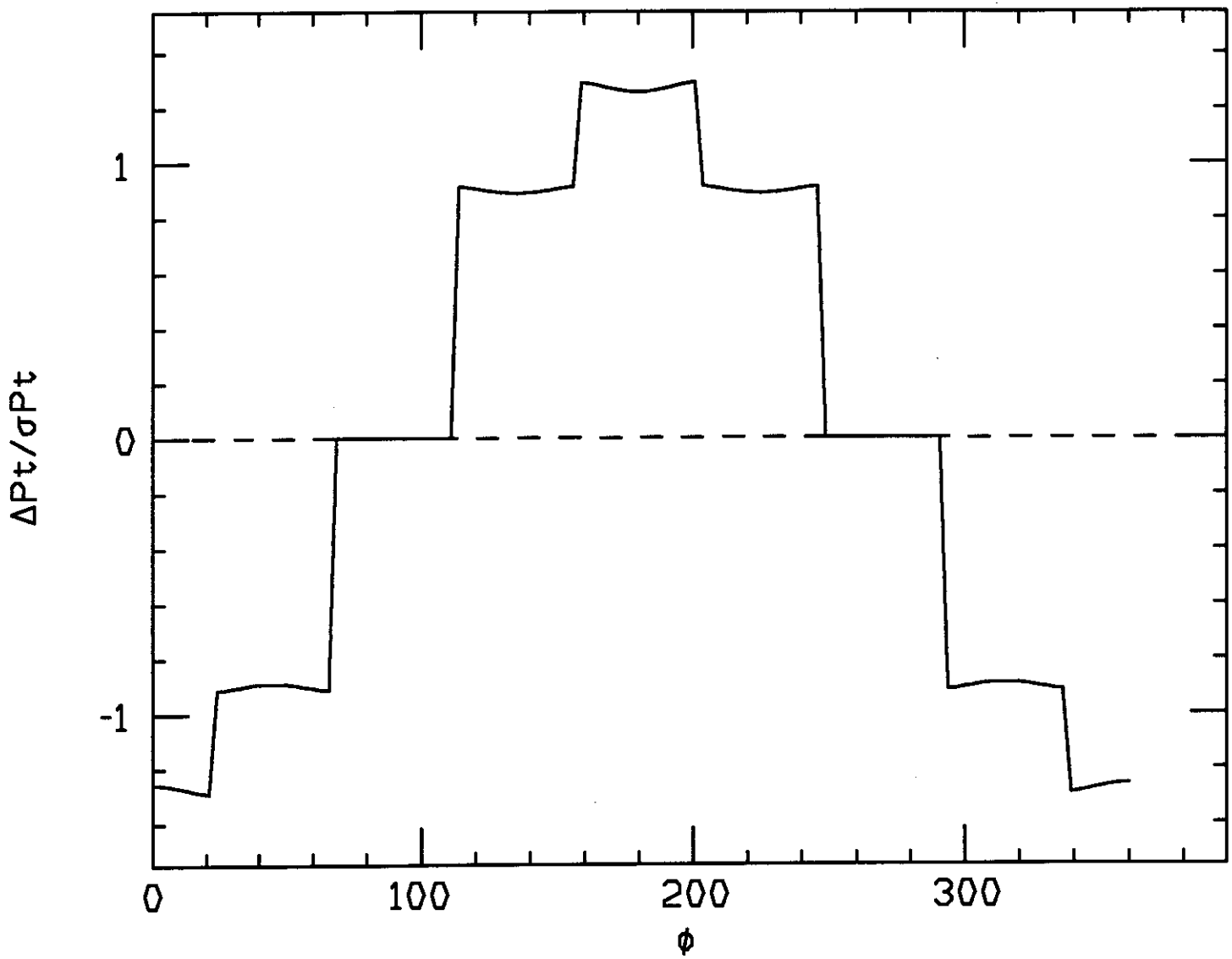
Figure 4 : Pt = 1000 GeV, η = 1.0